SDC-91-164

SDC
SOLENOIDAL DETECTOR NOTES

TWO DIMENSIONAL MAGNETIC ANALYSIS OF THE SOLENOIDAL DETECTOR FOR THE SUPERCONDUCTING SUPER COLLIDER

December 1991

T. Adams, M. Anderson and B. Easom
Martin Marietta Astronautics Group, Science Systems

SDC-91-164

Two Dimensional Magnetic Analysis of The Solenoidal Detector for the Superconducting Super Collider

Prepared by:

T. Adams, M. Anderson, B. Easom
Martin Marietta Astronautics Group, Science Systems

December 1991

SCIENCE SYSTEMS
MARTIN MARIETTA ASTRONAUTICS GROUP
DENVER, CO.

Foreword

This report has been prepared and is submitted by the Science Systems division of the Martin Marietta Astronautics Group to the Superconducting Super Collider Laboratory (SSCL) in accordance with Contract SSC-92-Z-16308.

This report describes the methods, results and conclusions of a two dimensional magnetostatic analysis performed to determine the level of magnetic fields within and surrounding the SDC detector for the purpose of assessing the operating environment for both personnel and equipment. Flux contributions from both the toroid and solenoid magnets are calculated.

Table of Contents

Sections — page

1.0 Introduction ____ 4
2.0 Analysis Approach ____ 5
3.0 Solenoid Magnet Analysis Model ____ 5
4.0 Toroid Magnet Analysis Model ____ 5
5.0 Conclusions ____ 6
6.0 References ____ 21

Figures

1 Schematic of Analysis Model Indicating the Locations of the Various Components. ____ 4
2 Finite element mesh for the SDC solenoid analysis model. ____ 7
3 End View of Barrel Calorimeter Illustrating the Azimuthal Distribution of End Cap/ Barrel Contact Areas and the Space Allocated for Routing Cables and Utilities. ____ 8
4 Relative Magnetic Permeability vs. Flux Density for A87 Steel. ____ 9
5 Magnetic Flux Density Contour Plot For the SDC Solenoid With the Gap Between Barrel and Endcap Calorimeters Modeled As Air. ____ 12
6 Magnified View of Magnetic Flux Density Contour Plot For the SDC Solenoid Showing Leakage from the Area Around the Air Gap. ____ 13
7 Magnified View of Magnetic Flux Density Contour Plot For the SDC Solenoid Showing the High Levels in the Area Very Near the Air Gap. ____ 14
8 Magnetic Flux Density Contour Plot For the SDC Solenoid With the Gap Between Barrel and Encap Calorimeters Modeled As Steel. ____ 15
9 Magnified View of Magnetic Flux Density Contour Plot For the SDC Solenoid Showing Leakage Near the Steel Contact Area. ____ 16
10 Barrel Toroid Conductor. ____ 17
11 Finite Element Mesh for the SDC Toroid Analysis Model. ____ 18
12 Contour Plot Of Magnetic Flux Density for the Air Surrounding the SDC Toroid. ____ 19
13 Magnified Contour Plot Of Magnetic Flux Density For the Air Within the SDC Toroid. ____ 20

Tables

1 Magnetic Properties of Materials (Linear). ____ 8
2 SDC Calorimeter Layup and Magnetic Permeability Stacking Factors. ____ 10
3 Steel B, H & μ_R Values for Non-Linear Analyses. ____ 11

Appendix A - Color Contour Plots ____ 22

1.0 Introduction

The detector design proposed by the Solenoidal Detector Collaboration (SDC) (Reference 1) for the Superconducting Super Collider uses two magnets to aid in particle identification and momentum resolution (Figure 1.). A superconducting solenoid will provide a uniform magnetic field of 2.0 tesla within the tracking volume for charged particle identification while a conventional octagon shaped iron core toroid will provide a nominal 1.8 tesla field within the toroid iron for muon identification and momentum resolution. A large calorimeter consisting of scintillating tiles sandwiched between absorber plates will reside within the toroid barrel. The electromagnetic sections of the calorimeter will use lead as the absorber medium while the hadronic sections will use steel. The hadronic sections of the barrel and endcap calorimeters will also provide a flux return path for the solenoid. The baseline design calls for mounting the photo multipliers and electronics associated with the tracking and calorimeter systems directly to the outside surface of the calorimeter, within the space provided between the calorimeter and toroid. This approach promises to minimize cable lengths and allows for access to a large portion of the detector electronics without major disassembly. The benefits thus gained in ease of access may, however, be offset by possible performance degradation and personnel safety concerns arising from the presence of extraneous magnetic fields. The purpose of this analysis is to calculate the magnitude and distribution of magnetic fields leaking from both the toroid and solenoid magnets during operation. The areas of greatest interest are those lying between the calorimeter outer surface and the toroid. Magnetic fields leaking from the detector into the hall are also calculated.

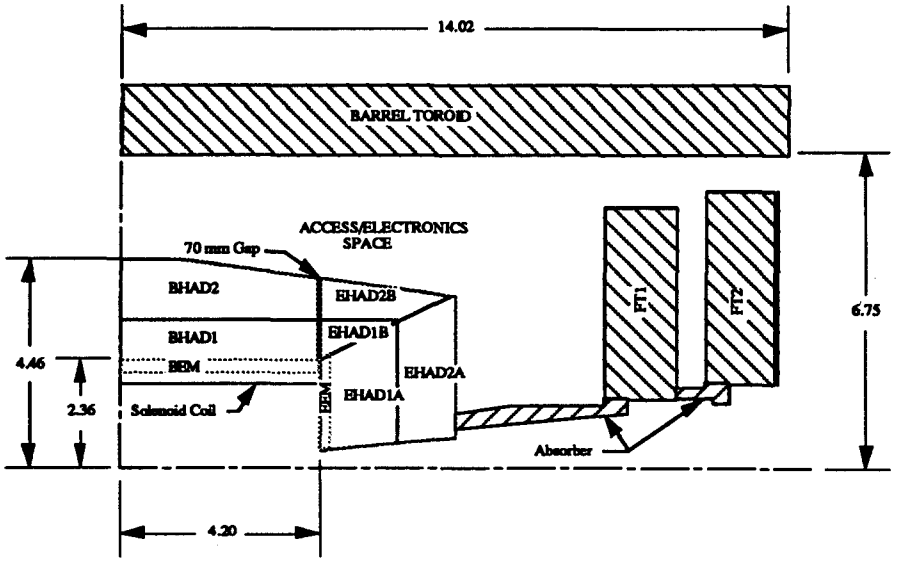

Figure 1 Schematic of Analysis Model Indicating the Locations of the Various Components (dimensions are meters).

2.0 Analysis Approach

This problem is really an ideal candidate for a three dimensional analysis since the fields for the solenoid and toroid are essentially perpendicular to one another and because the flux return path between the endcap and barrel calorimeters will probably vary around the circumference. Three dimensional analyses, however, tend to be rather involved and schedule constraints were such that a faster approach needed to be used. A relatively quick answer is obtained using separate, two dimensional, axi-symmetric models of the solenoid and toroid with the assumption that the relative contribution from one is small near the other. The validity of this assumption is bourne out during the course of the analysis.

We use MSC EMAS/XL (Reference 2), a commercially available FEM computer code capable of both two and three dimensional magnetic analyses including non-linear material effects such as saturation. The finite element models themselves are generated using the SDRC IDEAS SuperTab (Reference 3) pre & post-processing package which is also capable of writing an EMAS/XL input file. The calculations are then performed within EMAS and the results read back into SuperTab for display. This approach is used in order to take advantage of an existing geometry data base which was generated as part of an ongoing effort to develop a detailed solid model of the SDC detector. EMAS calculates values of magnetic vector potential (A) and so the boundary conditions are; A tangent is zero for outer boundaries and A normal is zero for axes of symmetry. Detailed discussions of the finite element models for the solenoid and toroid follow.

3.0 Solenoid Magnet Analysis Model.

The finite element mesh for the superconducting solenoid analysis model is shown in Figure 2. This model is comprised of ~1200 elements total. The elements defining the gap between the end cap and barrel calorimeters are grouped so that their magnetic properties can be easily changed from those of air, representing the space allocated for nonmagnetic cable routing, to those of steel, representing the annular contact areas separating adjoining cable spaces. The end view of the barrel calorimeter in Figure 3 depicts one possible distribution of the contact areas and cable space. The symmetric pattern is intended to minimize field distortions in the barrel-end cap contact area which could, in turn, adversely effect field uniformity within the tracking volume. Table 1 and Figure 4 provide values of relevant properties used for the various detector components in this analysis. Although the conductors for the the barrel and forward toroids are not modeled, the toroids are assumed to be operating at 1.8 tesla and as such are given relative permeabilities of 150 as indicated from the data of Figure 4. Stacking factors calculated for the calorimeter and provided in Table 2 indicate that the presence of the scintillator will result in a less than 10% reduction in overall permeability therefore we model the hadronic calorimeter as homogeneous steel. Analyses are conducted in the non-linear mode using the data for steel provided in Table 3. The superconductor is modeled as a 20 mm thick annulus with mean radius of 1810 mm carrying a uniform current density of 8.0e7 Amps/m^2 (Reference 6).

Analysis results are provided as contour plots of magnetic flux density in Figures 5 through 9.

4.0 Toroid Magnet Analysis Model.

An existing model was used for the toroid analysis. It was originally developed during the course of the muon barrel toroid trade study analysis (Reference 7) conducted for the SSCL in March 1991. The conductors carry 4,494 Amps and are modeled as a single uniform

conductor with dimensions as shown in Figure 10. The nominal operating field for the toroid is 1.8 tesla, which is near the saturation level for steel, therefore the toroid analysis was conducted in the EMAS non-linear mode. The conductors on the inside of the toroid for this model are located 24.6 cm from octant corner centerlines. Figure 11 shows the finite element mesh generated for the model, which is comprised of 528 elements.

Analysis results provided in Figures 12 and 13 indicate fields from the toroid near the calorimeter outside surface are between 5 and 10 gauss depending on axial location.

5.0 Conclusions

The analysis results indicate that magnetic field levels at the calorimeter surface near the gap between barrel and endcap can be as high as 1000 gauss for a continuous air filled gap and as low as 5 gauss for a steel filled gap. In reality, the presence of the steel contact areas should provide a preferred flux path and result in substantial reductions in leakage from the adjoining air gap areas. Three dimensional analyses are needed to more accurately determine how much the proposed steel contact areas will reduce leakage. The contour maps also show that the greatest levels of leakage fields are very highly localized near the gap, falling off rapidly with distance from it. Although it is possible to shield equipment, by either placing it away from the gap area or by surrounding it with soft iron and or mu-metal, it is not clear at the time of this report what level of shielding is needed or what can be obtained. Even if leakage from the solenoid is eliminated entirely there is still the 5 to 10 gauss contributed by the toroid. It is possible to minimize the toroid leakage by optimizing the placement of the coils relative to each other and to the octant corners. A two dimensional analysis should be adequate to identify the optimal geometry.

We recommend that the desired operating environments for phototubes, electronics and other sensitive equipment be defined by the users and that future analyses investigate three dimensional effects as necessary to assess the detector design against these requirements. Analyses should also be conducted to determine the levels of shielding necessary and wether they can be obtained at reasonable cost. We also recommend that an analysis be conducted to determine the optimum toroid coil positions to minimize fringe field effects.

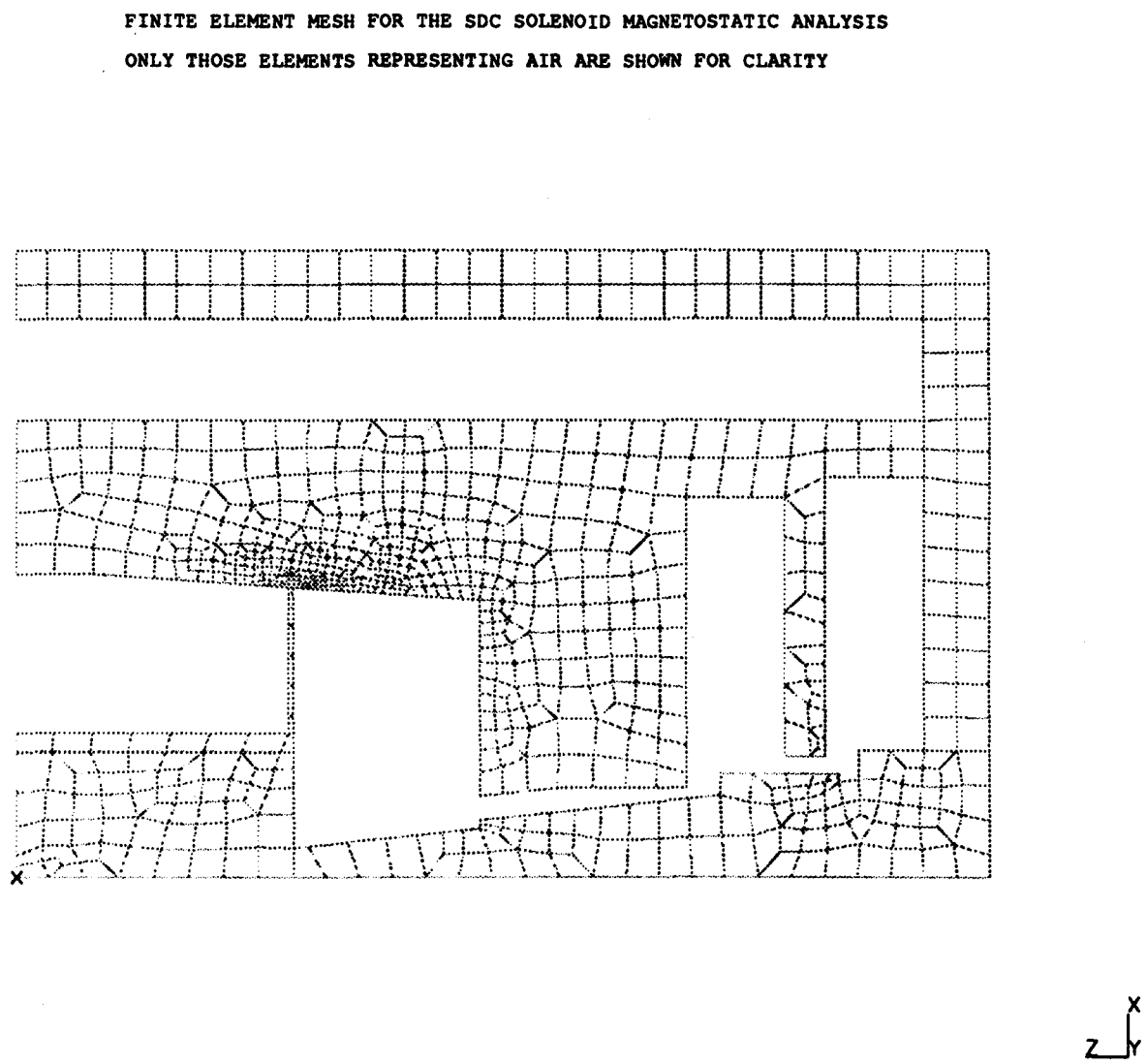

Figure 2 Finite element mesh for the SDC solenoid analysis model.

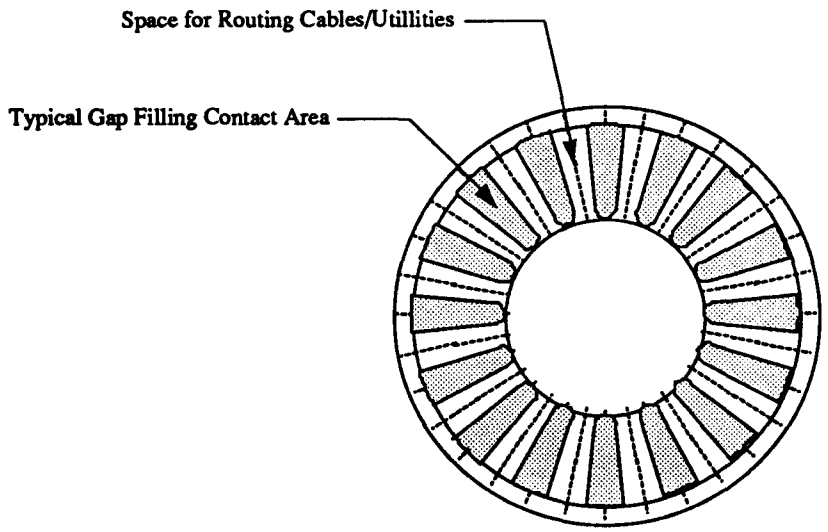

Figure 3 End View of Barrel Calorimeter Illustrating the Azimuthal Distribution of End Cap/ Barrel Contact Areas and the Space Allocated for Routing Cables and Utilities.

Table 1 Magnetic Properties of Materials (Linear).

Component	Relative Permeability	Conductivity
Solenoid Coil	1.0	1.0e15
Air	1.0	1.0e-9
Toroid Iron (1.8 Tesla)	150.	1.0e7
Absorber	10000.	1.0e7
End Cap HAC2A	9800.	1.0e7
End Cap EHAC1A	9500.	1.0e7
End Cap EM	1.0	1.0e7
End Cap HAC1B	9100.	1.0e7
End Cap HAC2B	9500.	1.0e7
Barrel EM	1.0	1.0e7
Barrel HAC1	9100.	1.0e7
Barrel HAC2	9500.	1.0e7
Barrel/Endcap Cal. gap		
Air	1.0	1.0e-9
Steel	10000.	1.03e7

See Figure 1 for the locations.

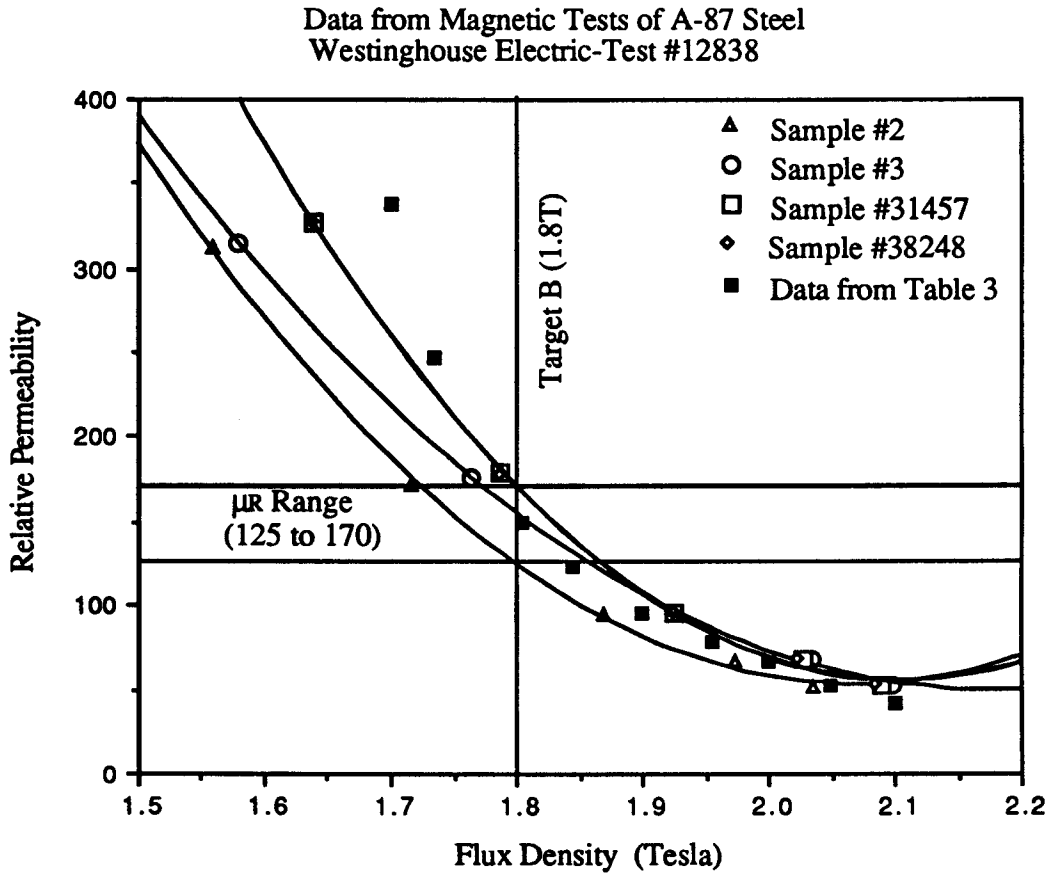

Figure 4 Relative Magnetic Permeability vs. Flux Density for A87 Steel (Reference 5).

Table 2 SDC Calorimeter Layup and Magnetic Permeability Stacking Factors*.

Barrel HAD1 & Encap HAD1B (BHAD1 & EHAD1B)

Abs. thickness (mm)	25.4 Fe
Scint. thickness (mm)	2.5
Absorber layers	32
Stacking Factor	.91

Barrel HAD2 & Endcap HAD2B (BHAD2 & EHAD2B)

Abs. thickness (mm)	51 Fe
Scint. thickness	2.5
Abs. layers	13
Stacking Factor	.95

Endcap HAD1A (EHAD1A)

Abs. thickness (mm)	51 Fe
Scint. thickness (mm)	2.5
Absorber layers	21
Stacking Factor	.95

Endcap HAD2A (EHAD2A)

Abs. thickness (mm)	102 Fe
Scint. thickness	2.5
Abs. layers	8
Stacking Factor	.98

*Calorimeter Configuration Data Provided by P. Mantch , FNAL, November 25 1991.

Table 3 Steel* B, H & μ_R Values for Non-Linear Analyses.

Flux Density (Tesla)	H (Amp/m)	Relative Permeability
0.00e+0	0.00e+0	1.00e+4
1.00e+0	2.95e+2	2.70e+3
1.10e+0	3.40e+2	2.57e+3
1.20e+0	4.00e+2	2.39e+3
1.30e+0	5.00e+2	2.07e+3
1.40e+0	6.00e+2	1.86e+3
1.45e+0	8.00e+2	1.44e+3
1.50e+0	9.60e+2	1.24e+3
1.55e+0	1.25e+3	9.87e+2
1.60e+0	1.62e+3	7.86e+2
1.64e+0	2.39e+3	5.48e+2
1.67e+0	3.18e+3	4.19e+2
1.70e+0	4.00e+3	3.38e+2
1.73e+0	5.57e+3	2.48e+2
1.81e+0	9.54e+3	1.51e+2
1.85e+0	1.19e+4	1.23e+2
1.90e+0	1.59e+4	9.50e+1
1.96e+0	1.99e+4	7.82e+1
2.00e+0	2.40e+4	6.63e+1
2.05e+0	3.10e+4	5.26e+1
2.10e+0	4.00e+4	4.18e+1

* Values given are for JIS SS41 steel from Reference 8

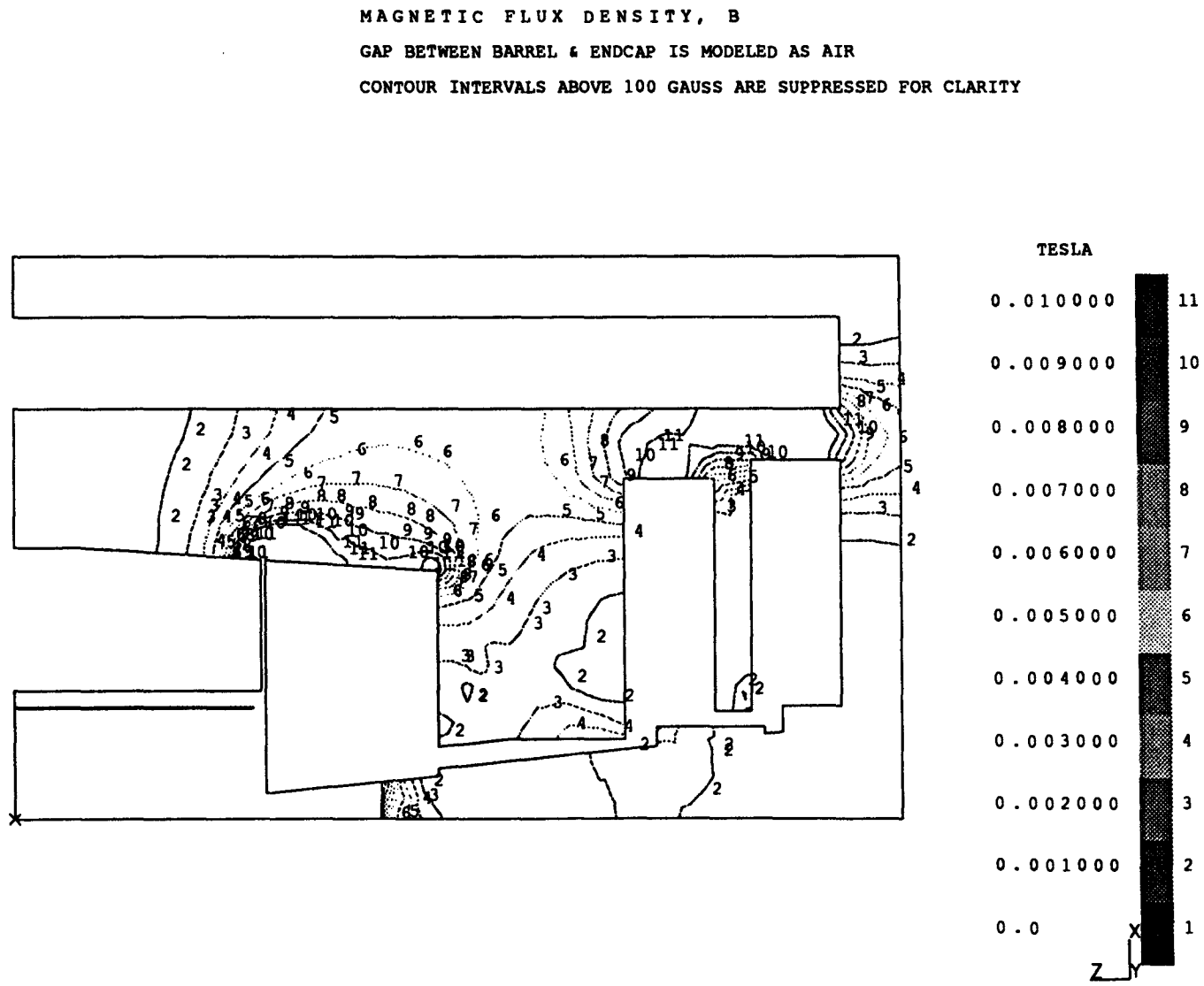

Figure 5 Magnetic Flux Density Contour Plot For the SDC Solenoid With the Gap Between Barrel and Encap Calorimeters Modeled As Air.

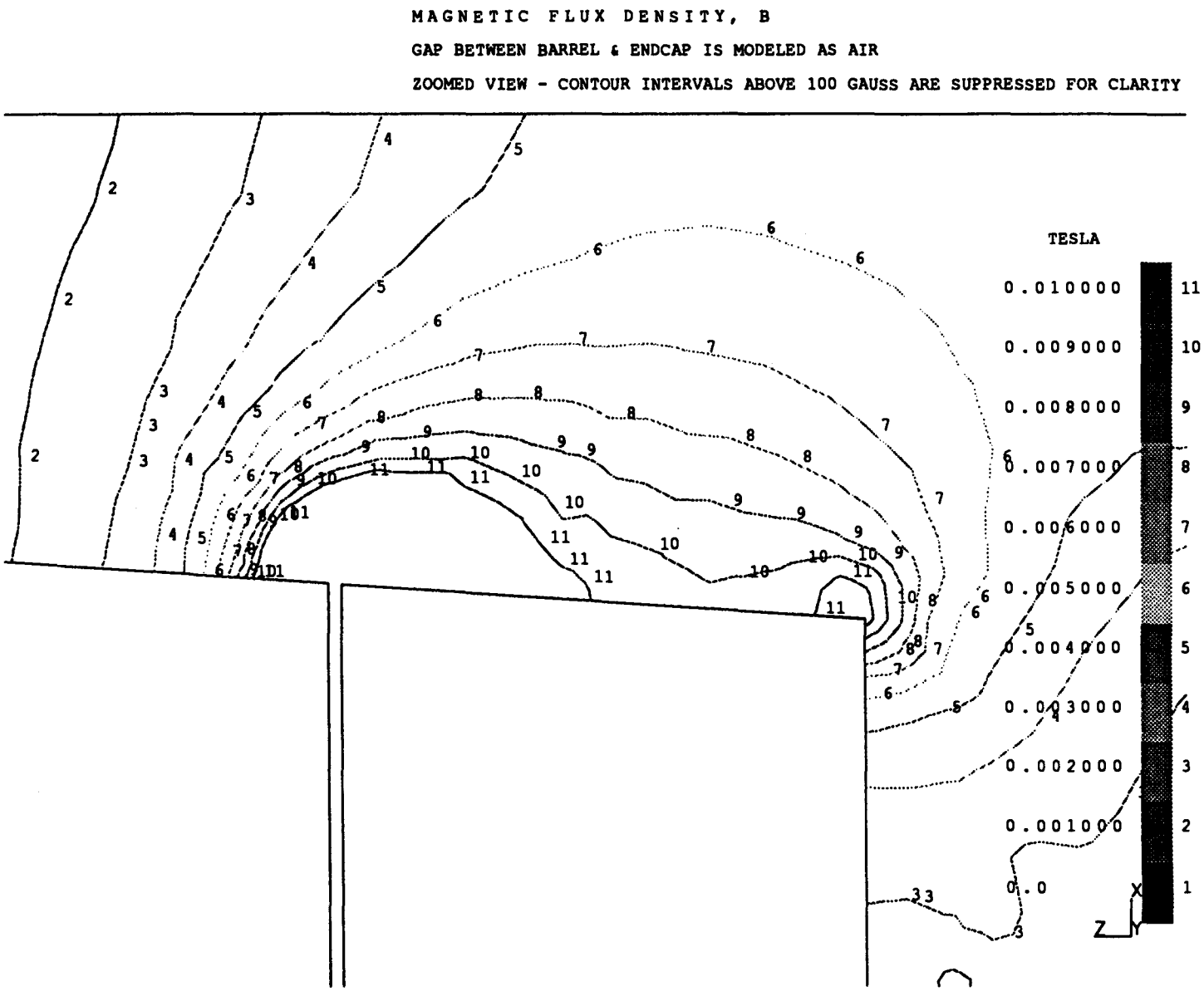

Figure 6 Magnified View of Magnetic Flux Density Contour Plot For the SDC Solenoid Showing Leakage from the Area Around the Air Gap.

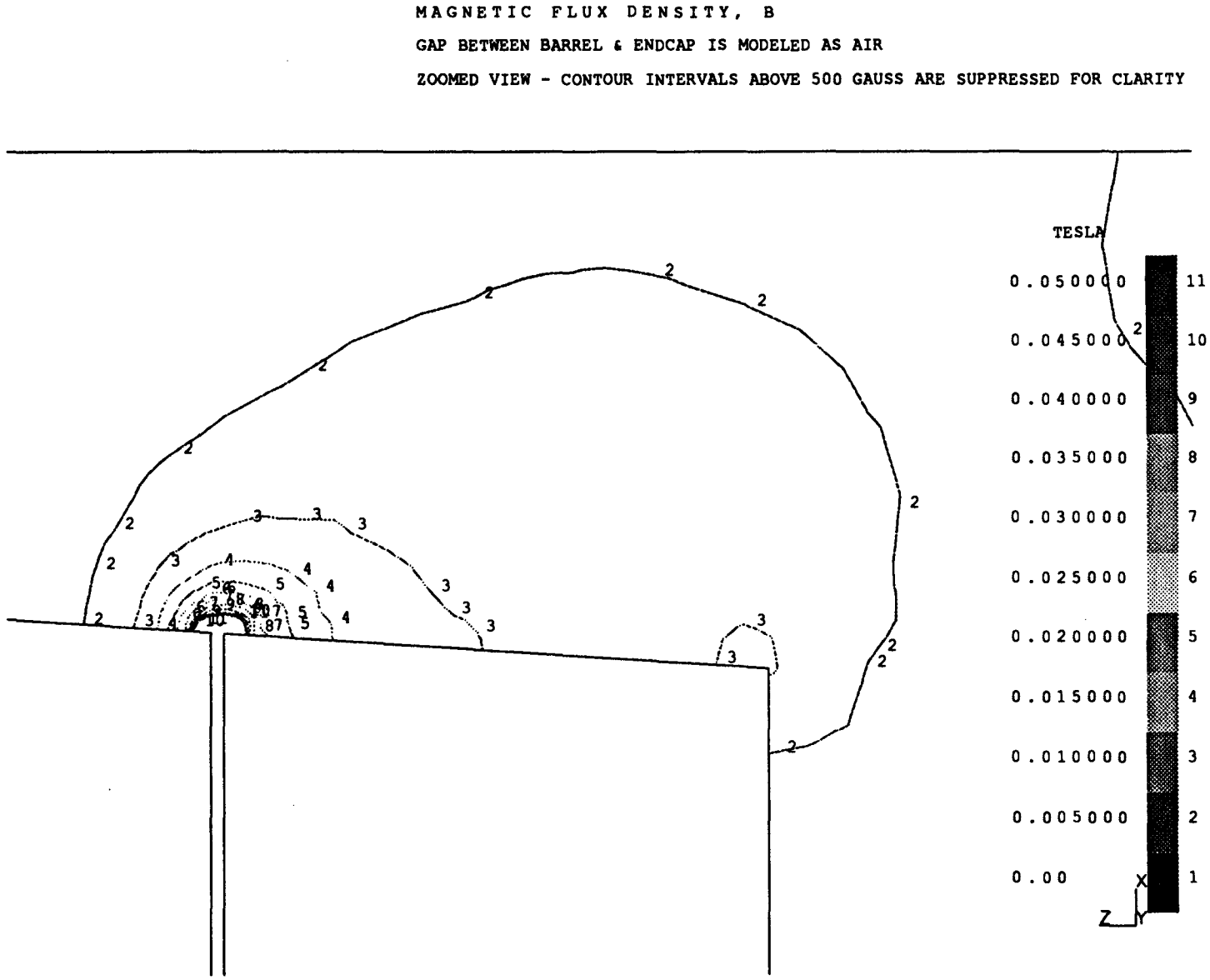

Figure 7 Magnified View of Magnetic Flux Density Contour Plot For the SDC Solenoid Showing the High Levels in the Area Very Near the Air Gap.

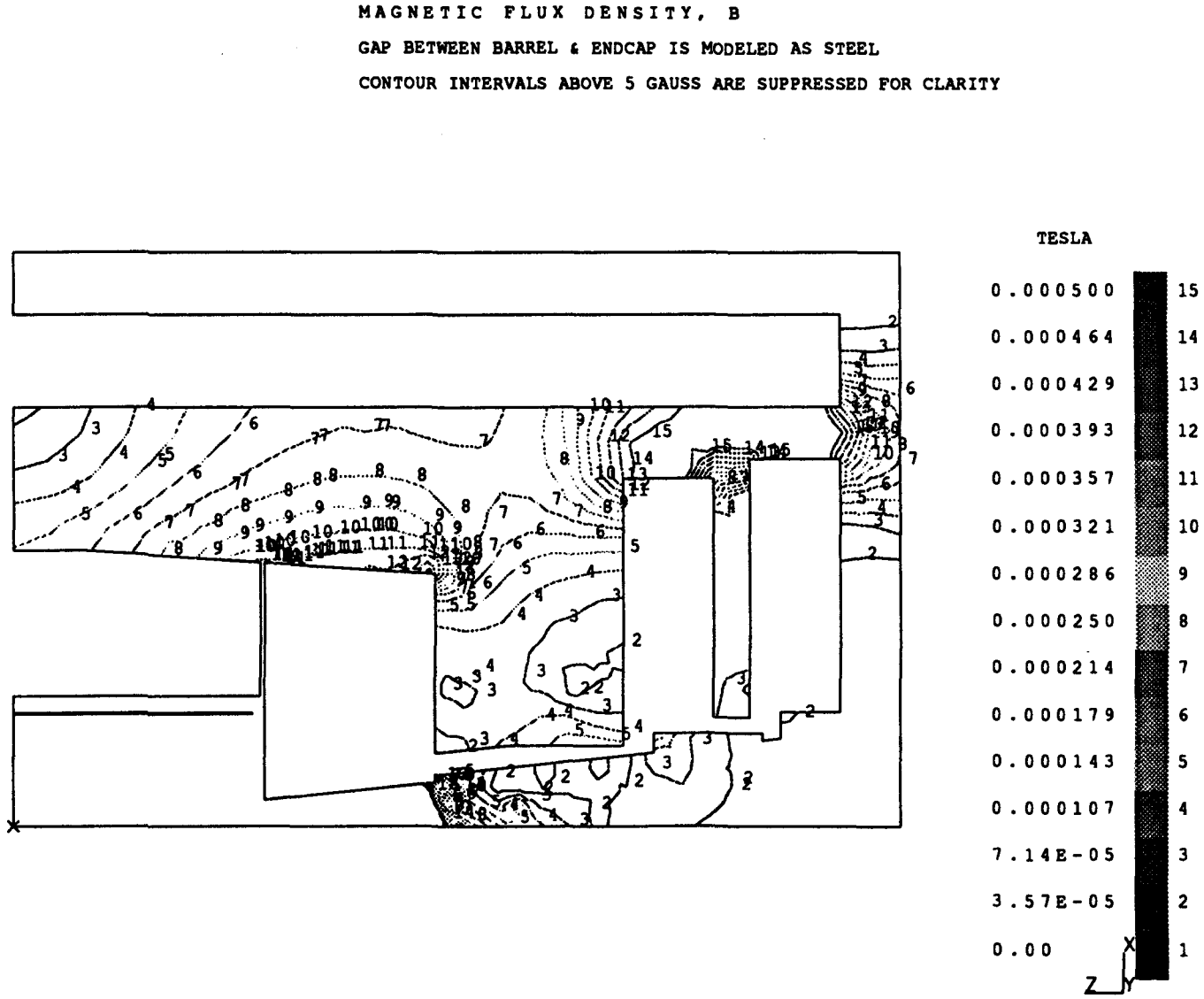

Figure 8 Magnetic Flux Density Contour Plot For the SDC Solenoid With the Gap Between Barrel and Encap Calorimeters Modeled As Steel.

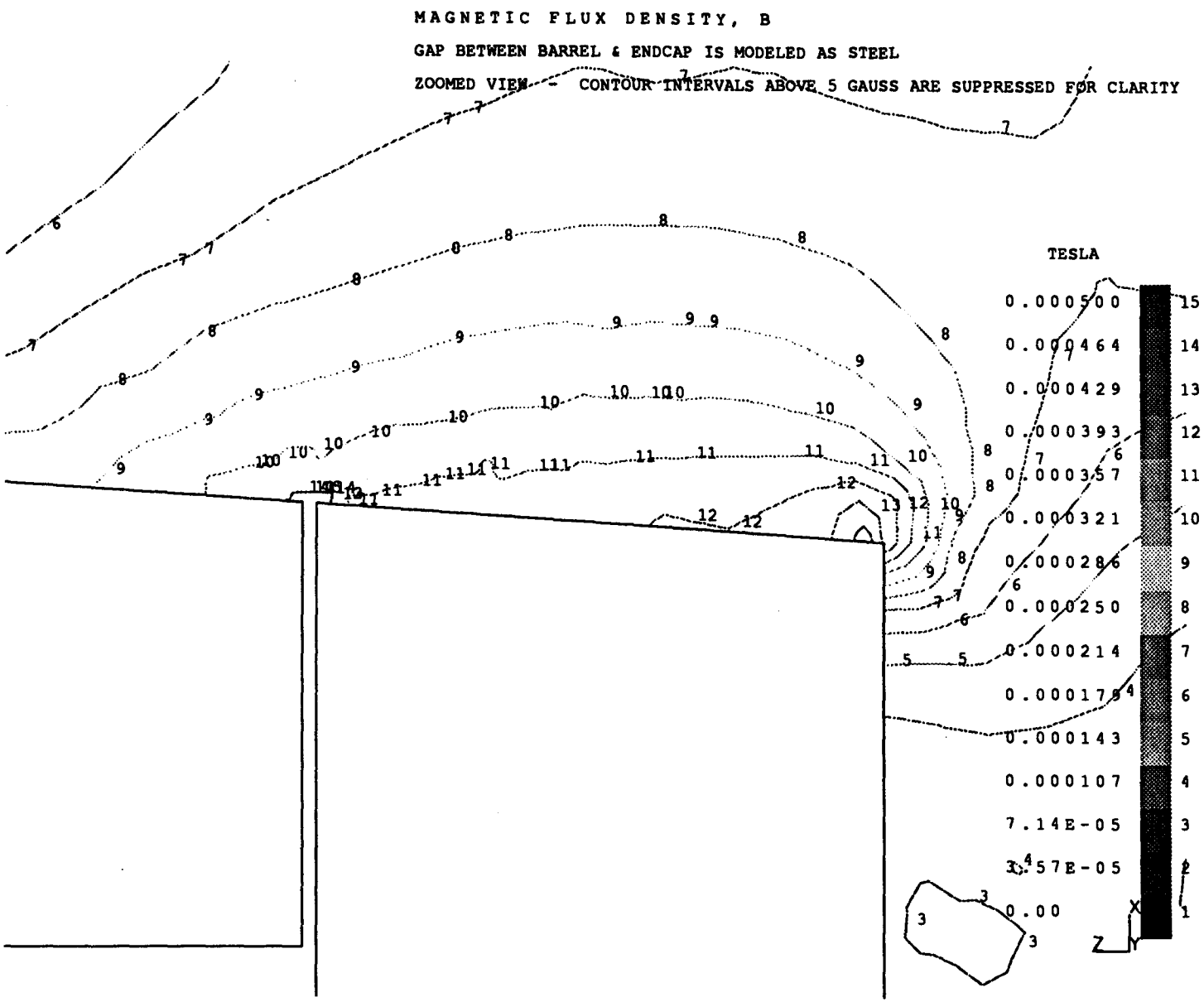

Figure 9 Magnified View of Magnetic Flux Density Contour Plot For the SDC Solenoid Showing Leakage Near the Steel Contact Area.

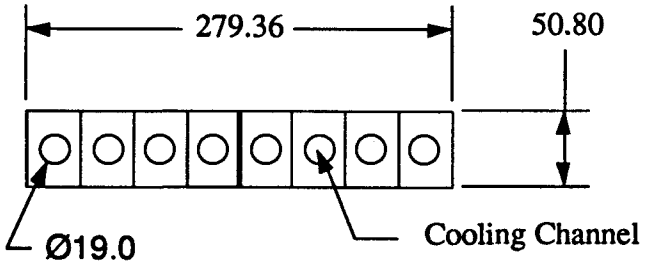

Figure 10 Barrel Toroid Conductor (dimensions are mm).

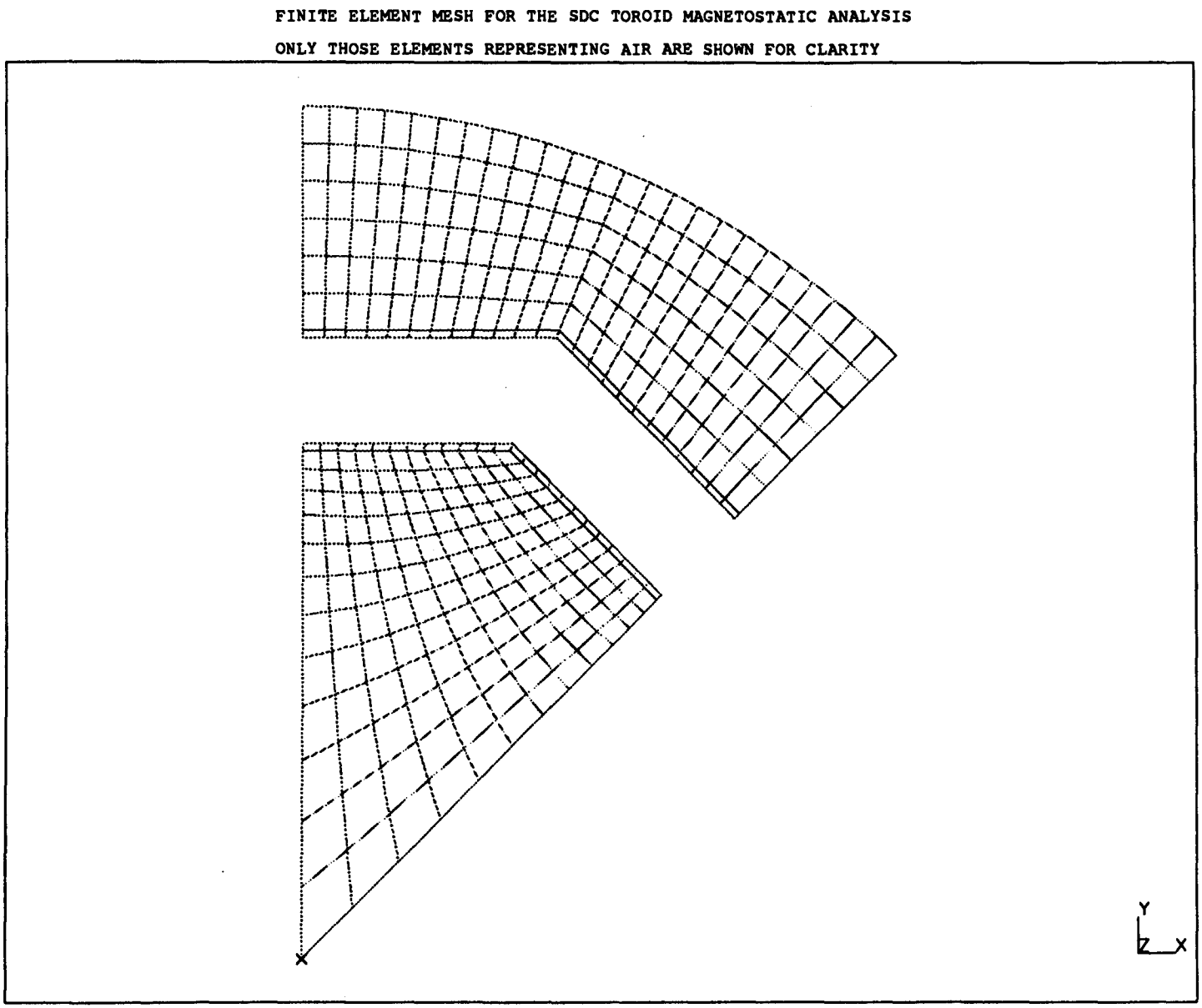

Figure 11 Finite Element Mesh for the SDC Toroid Analysis Model.

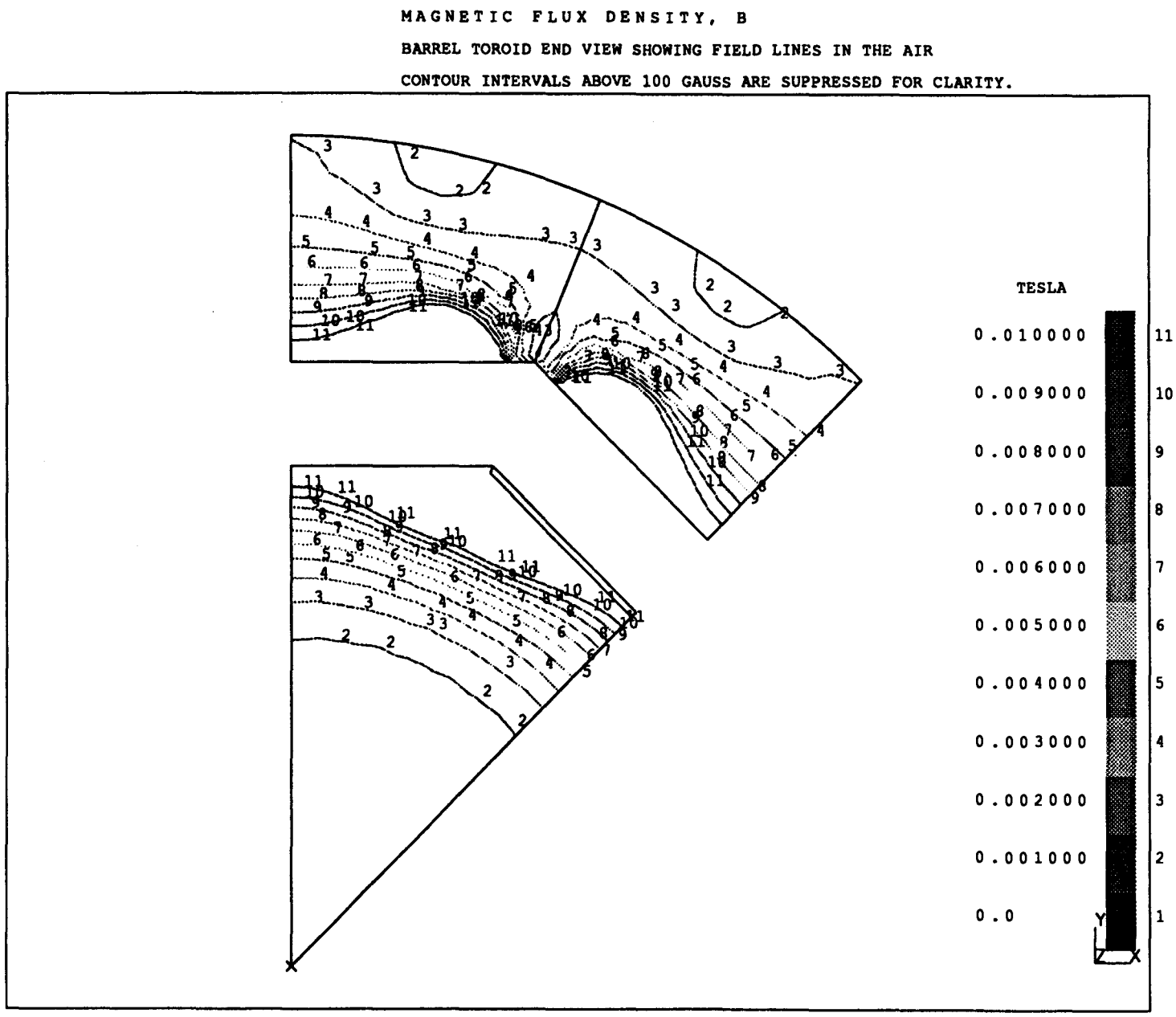

Figure 12 Contour Plot Of Magnetic Flux Density for the Air Surrounding the SDC Toroid.

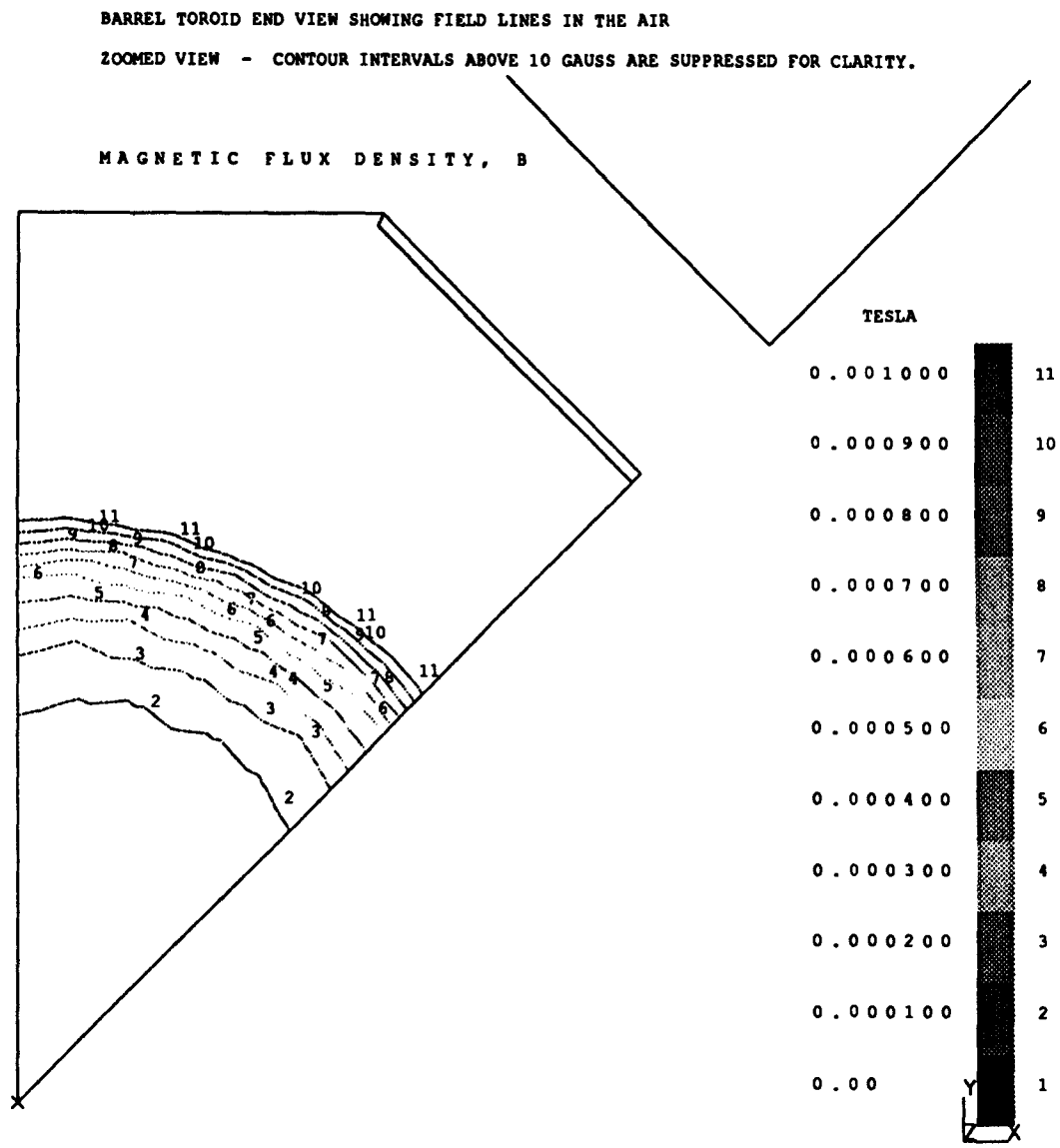

Figure 13 Magnified Contour Plot Of Magnetic Flux Density For the Air Within the SDC Toroid.

6.0 References

1.0 Letter of Intent by the Solenoidal Detector Collaboration, SDC-90-00151, 30 November 1990.

2.0 Electromagnetic Analysis System, MACNEAL-Schwindler Corporation, 4300 West Brown Deer Road, Suite 300, Milwaukee, Wisconsin 53223-2465, July 1991.

3.0 I-DEAS, Structural Dynamics Research Corporation, Milford, Ohio.

4.0 SDC Detector Parameters - Draft for Technical Board Review, SDT-000010, December 6, 1991.

5.0 SDC Muon Barrel Toroid Conceptual Design Report Using Long and Short Bolted Blocks,SDC Note: SDC-91-105, Jeff Cherwinka, September 25, 1991.

6.0 E-mail message from B. Wands (FNAL) to T. Adams, received November 22, 1991.

7.0 SDC Muon Steel Trade Study Evaluation, T.Adams *et al.*, SSC-91-Z-11103, March 31, 1991.

8.0 A. Maki *et al.*, Conceptual Design Studies of the SDC Iron Toroid System (I), December, 1990, KEK, National Laboratory for High Energy Physics.

APPENDIX A

COLOR CONTOUR PLOTS

MAGNETIC FLUX DENSITY, B

GAP BETWEEN BARREL & ENDCAP IS MODELED AS AIR

CONTOUR INTERVALS ABOVE 100 GAUSS ARE SUPPRESSED FOR CLARITY

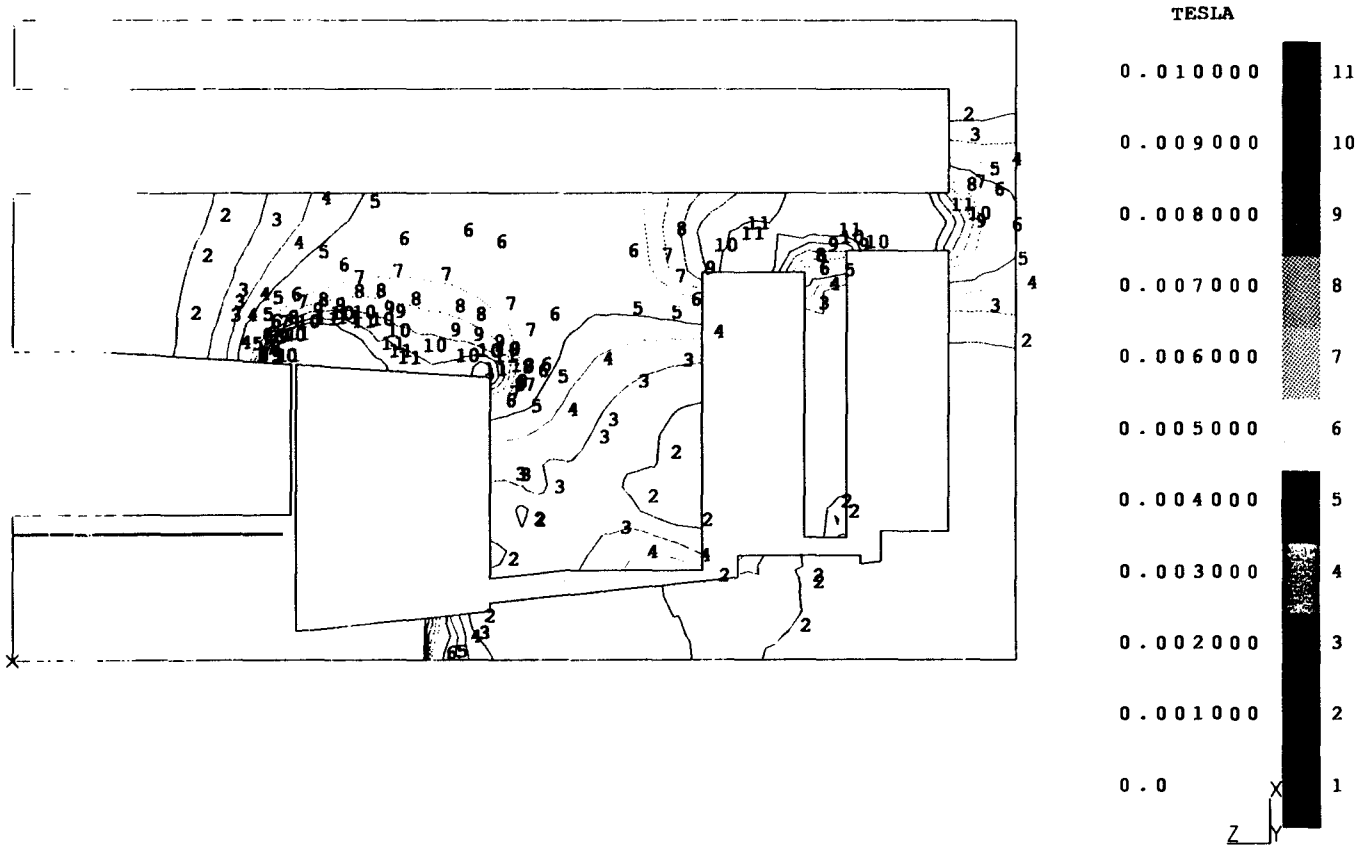

MAGNETIC FLUX DENSITY, B

GAP BETWEEN BARREL & ENDCAP IS MODELED AS AIR

ZOOMED VIEW - CONTOUR INTERVALS ABOVE 100 GAUSS ARE SUPPRESSED FOR CLARITY

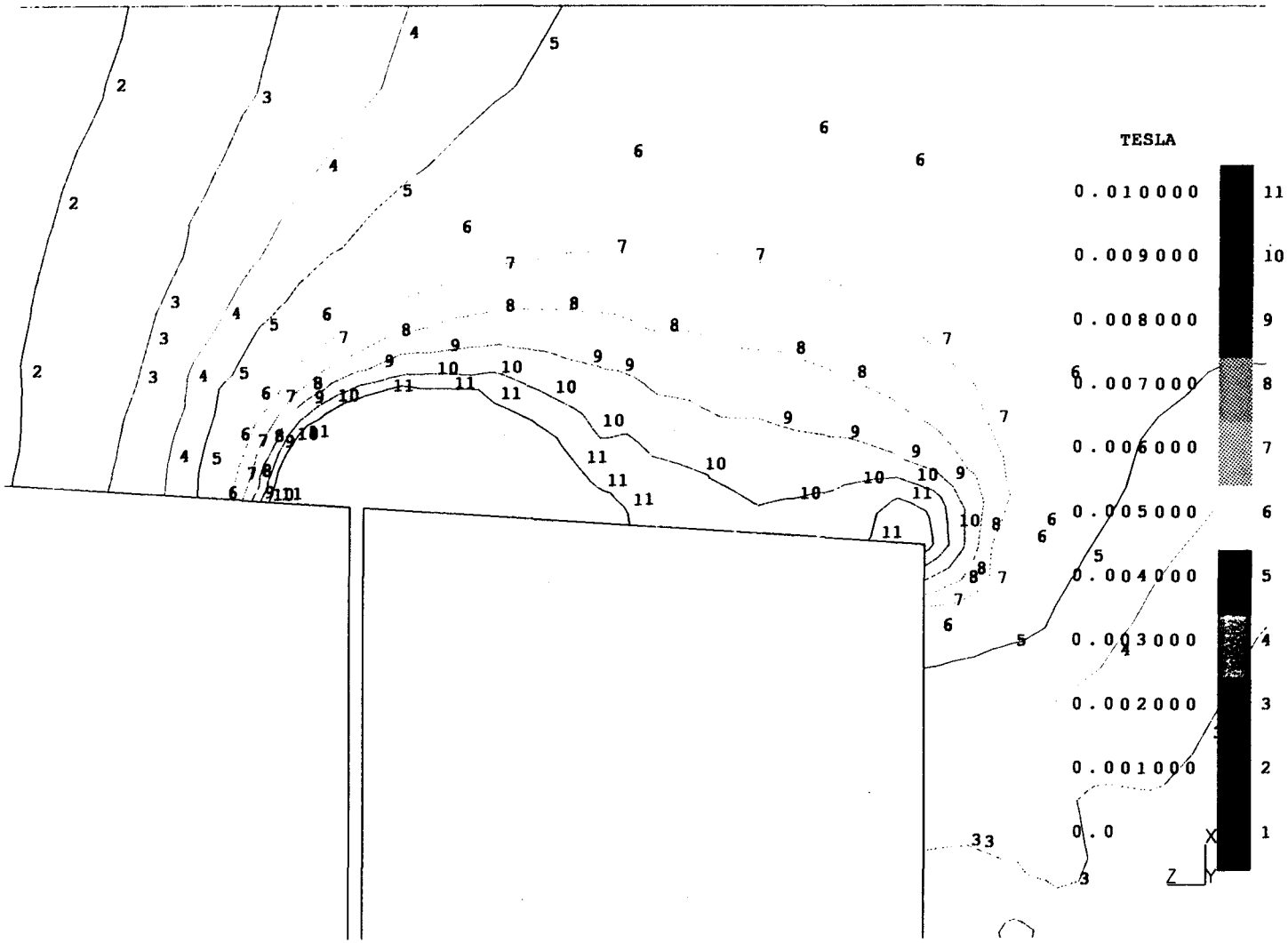

MAGNETIC FLUX DENSITY, B

GAP BETWEEN BARREL & ENDCAP IS MODELED AS AIR

ZOOMED VIEW - CONTOUR INTERVALS ABOVE 500 GAUSS ARE SUPPRESSED FOR CLARITY

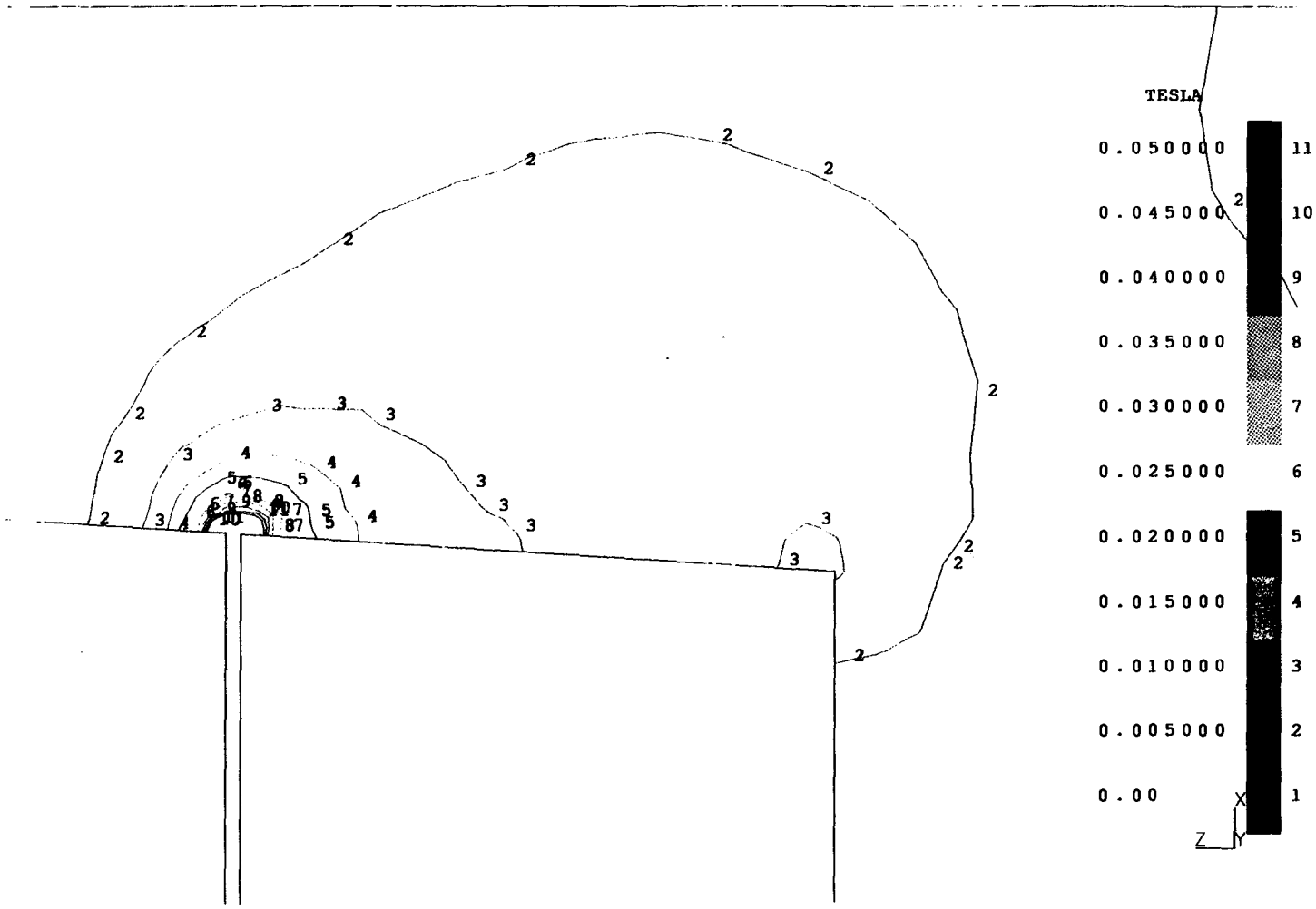

MAGNETIC FLUX DENSITY, B

GAP BETWEEN BARREL & ENDCAP IS MODELED AS STEEL

CONTOUR INTERVALS ABOVE 5 GAUSS ARE SUPPRESSED FOR CLARITY

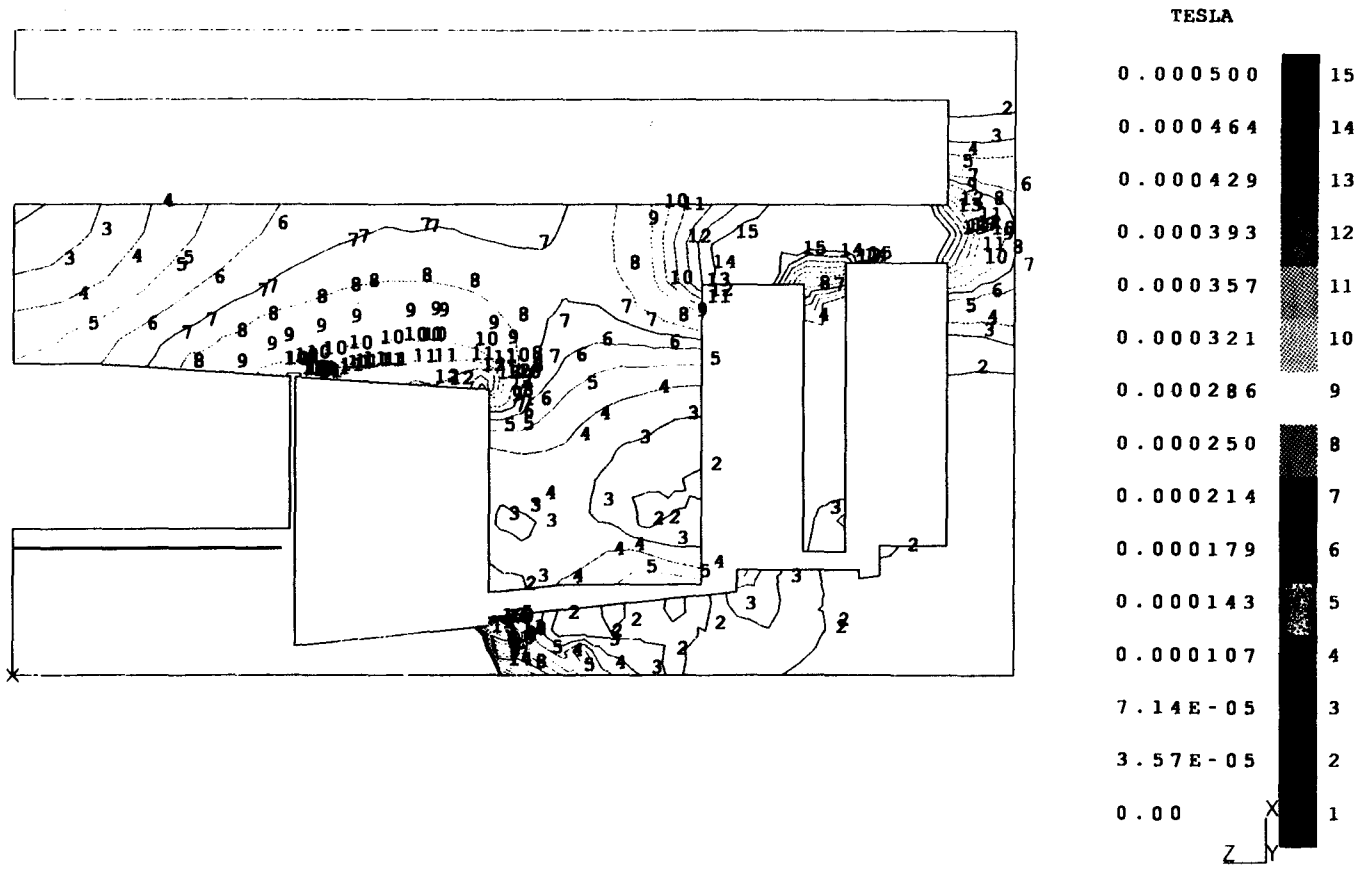

MAGNETIC FLUX DENSITY, B

GAP BETWEEN BARREL & ENDCAP IS MODELED AS STEEL

ZOOMED VIEW - CONTOUR INTERVALS ABOVE 5 GAUSS ARE SUPPRESSED FOR CLARITY

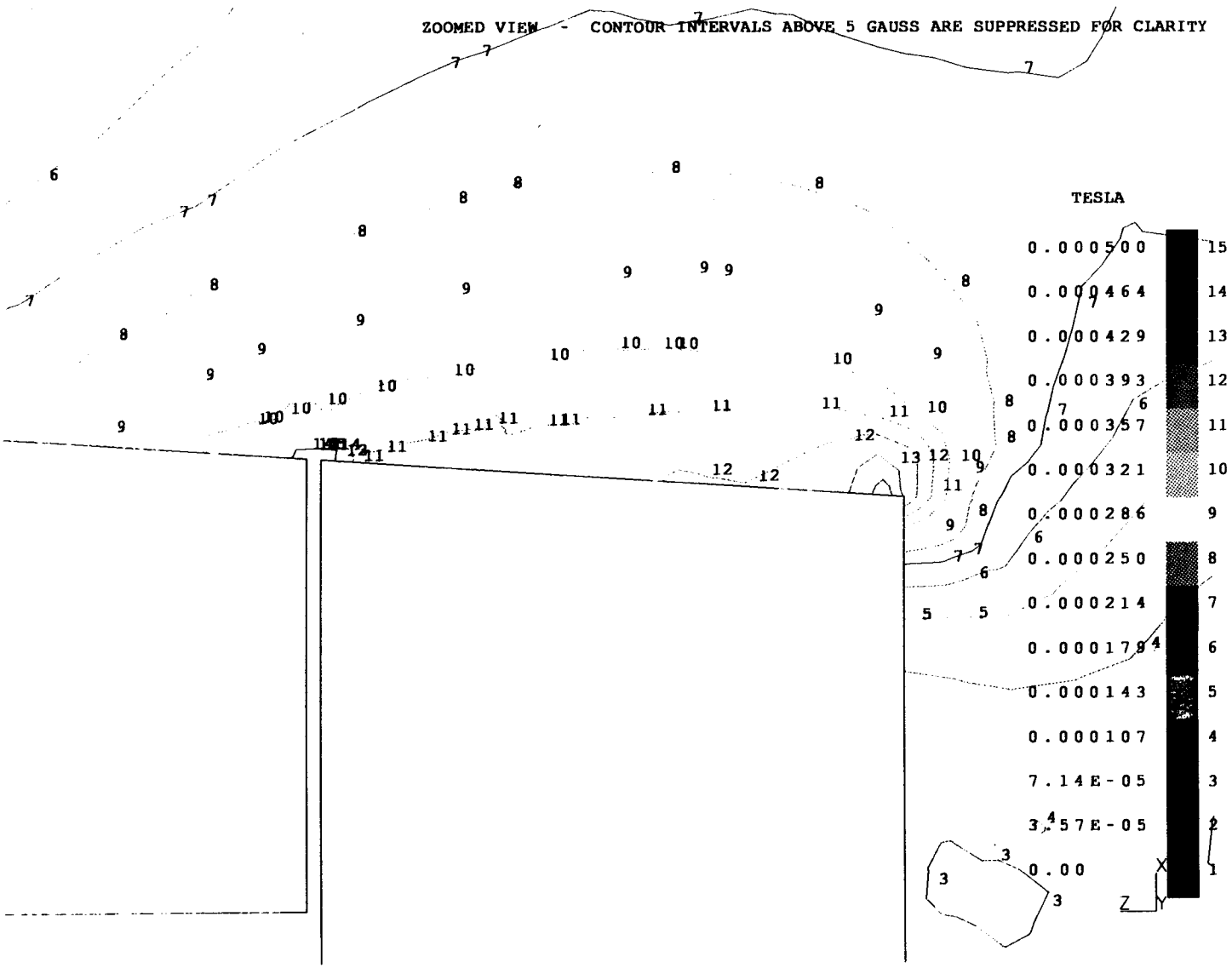

MAGNETIC FLUX DENSITY, B

BARREL TOROID END VIEW SHOWING FIELD LINES IN THE AIR

CONTOUR INTERVALS ABOVE 100 GAUSS ARE SUPPRESSED FOR CLARITY.

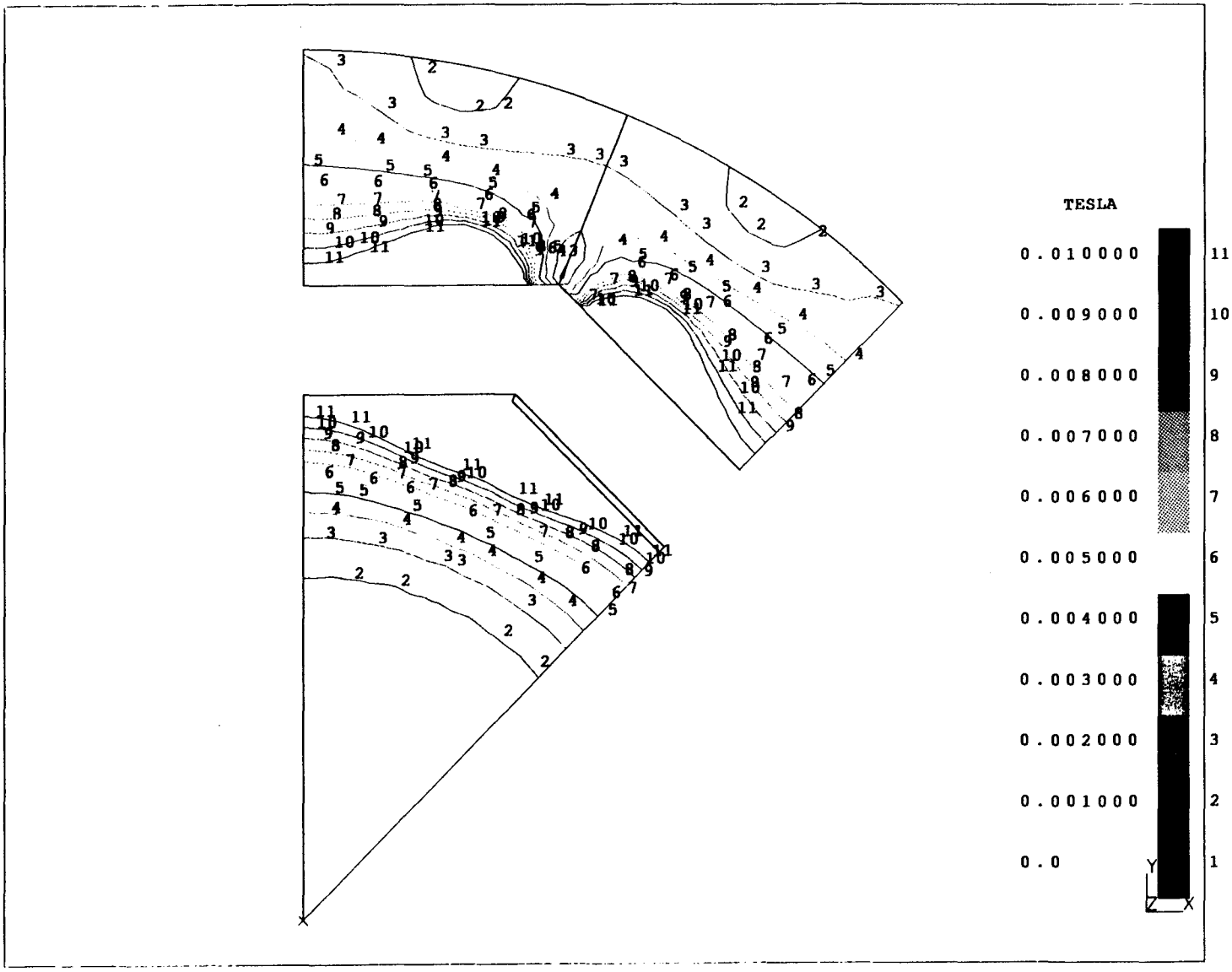

BARREL TOROID END VIEW SHOWING FIELD LINES IN THE AIR

ZOOMED VIEW - CONTOUR INTERVALS ABOVE 10 GAUSS ARE SUPPRESSED FOR CLARITY.
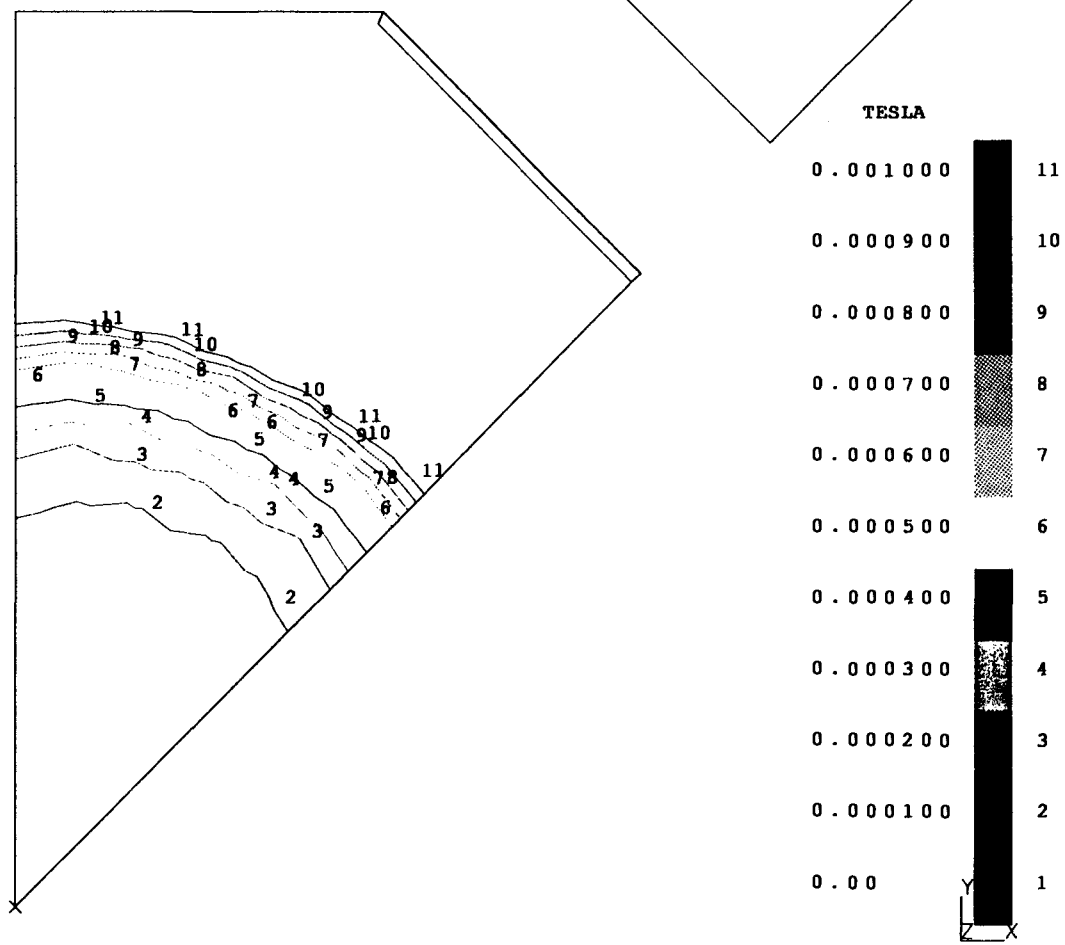
MAGNETIC FLUX DENSITY, B